Surface & Coatings Technology 432 (2022) 128036

Contents lists available at ScienceDirect

Surface & Coatings Technology

journal homepage: www.elsevier.com/locate/surfcoat

Influence of WC/C target composition and bias potential on the structure-mechanical properties of non-reactively sputtered WC coatings

T. Glechner [a,*], C. Tomastik [b], E. Badisch [b], P. Polcik [c], H. Riedl [a]

[a] Institute of Materials Science and Technology, TU Wien, A-1060 Wien, Austria
[b] AC2T Research GmbH, A-2700 Wiener Neustadt, Austria
[c] Plansee Composite Materials GmbH, D-86983 Lechbruck am See, Germany

ARTICLE INFO

Keywords:
Tungsten carbide
Magnetron sputtering
Crystal structure
Morphology
DFT

ABSTRACT

Physical vapor deposited WC based coatings strongly vary in their microstructure ranging from multi-phased columnar-crystalline up to nanocomposite coatings in relation to the usage of reactive or non-reactive carbon sources. Within this study, we investigated in detail the influence of additional carbon implemented into WC based target mmaterials as well as bias potential on the structure-mechanical properties of non-reactively sputtered WC coatings. Providing additional graphitic carbon within WC targets promotes the formation of nanocrystalline morphologies. Increasing bias potentials dominate the transition from a nanocrystalline to a columnar-crystalline morphology obtaining also a mixed state in between. The change in morphology is accompanied by a large modification in mechanical properties with hardness values ranging from 27 to 39 GPa, respectively. In addition, high adatom mobility – caused by bias potentials up to −200 V – predominates the phase formation of crystalline WC coatings changing from face-centered cubic (fcc)-WC_x to competing W_2C based structures. The W—C phase formation is furthermore examined using DFT calculations.

1. Introduction

Various tribological as well as machining applications (e.g. steels and alloys) require coating materials with characteristic properties. Physical vapor deposited (PVD) tungsten carbide (WC) is a widely used coating material due to its high hardness, specific tribological properties, as well as chemical inertness [1–4]. To further increase the multi-functionality of transition metal-carbide based coatings towards i.e. lower friction and higher toughness diverse concepts such as metastable structures, multilayered, gradient or nanocomposite coatings are applied [5–7]. In particular, the concept of nanocomposite coatings consisting of crystallites embedded in an amorphous matrix has been in focus in various studies reported in [8]. The bonding nature, crystallite size, and amount of predominant phases determine the properties of nanocomposite thin film materials [7,9]. It has been shown, that hardness can be enhanced for i.e. TiC/a-C:H nanocomposite coatings, while maintaining a low friction coefficient [10]. In a recent study, nanocomposite WC-coatings have been proven to exhibit a similar fracture toughness of 3.2 ± 0.24 $MPa{\cdot}m^{1/2}$ ($WC_{0.78}$) compared to a crystalline $WC_{0.67}$ coating [11]. In literature various PVD based methods are described for growing WC or WC-DLC based coatings, applying different target materials (W [1,12–14], WC [15], WC + Co [16,17], or additional pure C [6]) in reactive (C_2H_2, CH_4) as well as non-reactive (Ar) atmospheres. However, to gain a nanocomposite morphology either a reactive gaseous carbon source, requiring higher safety precautions, or an additional carbon target is needed. Another approach is to use targets with excess carbon built-into target material. However, this has yet been only reported for TiC [5], where a friction reduction could be achieved. For all deposition methods, a well-defined process stability and verifiable structures as well as morphology are highly desired.

Tungsten carbide has a further characteristic feature – making it specific in the deposition process – which are various competing stable and metastable phases. In detail, W_2C exists in three different modifications – orth-W_2C (Space group (SG) 60), hex-W_2C (SG 162, SG 194 [18]), next to metastable fcc-WC_x (SG 225) [16] and hexagonal (hex)-WC [19] (SG 187). During the deposition of WC based coating materials, often a mixture of fcc-WC_x and W_2C forms, which is reported to be influenced also by the applied bias voltage [14,20]. Furthermore, carbon deficiencies are very likely due to scattering with heavy atoms in the vapor phase (i.e. Ar or transition metal (TM)). Hence, when sputtering monocarbide targets (e.g. WC, TaC) the resulting coating is a sub-stoichiometric TM carbide [21]. For W—C but also Ta—C this

* Corresponding author.
E-mail address: thomas.glechner@tuwien.ac.at (T. Glechner).

https://doi.org/10.1016/j.surfcoat.2021.128036
Received 19 October 2021; Received in revised form 10 December 2021; Accepted 17 December 2021
Available online 25 December 2021

phenomenon is intensified through the strong tendency to form TM_2C based structures (W_2C, Ta_2C [22]). To counteract the carbon loss, excess carbon within the target materials is an interesting approach.

Therefore, within this study we investigated in detail the influence of additional carbon as well as bias potential on the structure-mechanical properties of non-reactively sputter deposited WC coatings. To vary the carbon content three different target materials, pure WC, WC/C (90/10 mol%), as well as WC/C (70/30 mol%) are used. Furthermore, we correlate the morphology with mechanical properties and further investigate the phase formation with the help of DFT calculations.

2. Experimental details

For the deposition of the tungsten carbide thin films, we used an in-house built magnetron sputter deposition system [11]. We used three different round 3-in. targets, a ceramic WC and two ceramic WC targets with additional graphitic carbon (10 and 30 mol%) added (Plansee Composite Materials GmbH). All targets were sputtered in DC mode with a target current of 0.55 A in pure argon atmosphere at a total pressure of 0.6 Pa. The target and the substrate holder were aligned parallel at a distance of 73 mm and a substrate temperature of 500 °C was used. The substrate bias was varied between floating potential and −200 V. In detail for the WC target we used floating, −65, −75, and −100 V; for the WC/C (90/10) target floating, −75, −100, and −125 V; whereas for the WC/C (70/30) target floating, −100, −150, and −200 V. All thin films were deposited on polished austenitic stainless-steel platelets (20 × 7 × 0.8 mm^3). Prior coating, the substrates were cleaned from contaminations in an ultrasonic bath by means of ethanol and acetylene. Furthermore, the target and the substrates were sputter-cleaned in a pure argon atmosphere right before the deposition.

To investigate the structure of the thin films, we used X-ray diffraction (XRD) in Bragg Brentano configuration applying a Panalytical Empyrean diffractometer equipped with a Cu-K_α radiation source (wavelength $\lambda = 1.54$ Å). The mechanical properties, such as hardness and indentation modulus, were determined on austenitic steel substrates by nanoindentation using an Ultra-Micro-Indentation System (UMIS) equipped with a Berkovich diamond tip. For every sample, 30 indents with different applied loads (3 to 45 mN) were performed. The respective load-displacement curves were analyzed after Oliver and Pharr [23]. The morphology was studied by transmission electron microscopy (TEM FEI TECNAI G20, acceleration voltage of 200 kV).

X-ray photoelectron spectroscopy (XPS) data were acquired using a Thermo Fisher Scientific Thetaprobe with a monochromatic Al Kα X-ray source (1486.6 eV) and a base pressure of 10^{-10} mbar. Immediately before entering the samples into the instrument, the samples were cleaned by wiping the surface with ethanol. Prior to analysis, surface contaminations on the samples were removed in situ by sputtering with 3 keV Ar ions. The high-resolution spectra of W, C and O were obtained at a pass energy of 50 eV, with an analysis spot size of 400 µm diameter. Spectrum evaluation was performed with the Thermo Fisher Scientific Advantage software, using Gaussian/Lorentzian peak fitting. The C 1s peak for adventitious carbon at 284.6 eV was used as binding energy reference.

3. Computational details

Density Functional Theory (DFT) calculations were performed using the VASP code (Vienna Ab Initio Simulation Package) [24], applying the projector-augmented plane-wave (PAW) pseudopotentials [25]. As exchange-correlation (xc) potential, we chose the Perdew-Burke-Ernzerhof Generalized Gradient Approximation (GGA-PBE) [26]. We compared four different W—C structures most commonly reported in literature: WC_x #SG 225, WC #SG 187, W_2C #SG 60 and W_2C #SG 162. We created a 2 × 2 × 2 supercell for WC_x as well as both W_2C structures, whereas a 3 × 3 × 3 supercell is used for hexagonal WC. We varied the C/W ratio by introducing carbon vacancies for hex-WC and WC_x, by filling up the partially occupied carbon sites for W_2C #SG 162, as well as by putting carbon atoms on interstitial sites for W_2C #SG 60, respectively. This was done using the Special Quasi-random Structure (SQS) method [27]. Equilibrium lattice parameters and ground-state energies were obtained by relaxing the supercell volumes, shapes and atomic positions (ISIF = 3 tag in VASP).

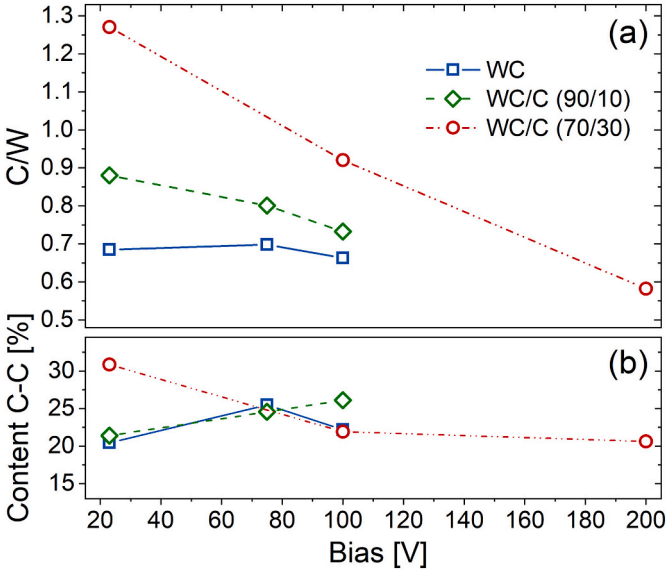

Fig. 1. Carbon to tungsten ratio with respect to the bias voltage and the target type (a). Amount of carbon which is present as amorphous C—C bonded carbon in the films (b). Data was obtained by XPS measurements.

4. Results and discussion

4.1. Chemical and structural analysis

The coatings deposited varied in thickness from 1.9 to 3.0 µm, where the deposition rate raised with increasing additional graphitic carbon in the target – 40 nm/min to 52 nm/min, for 0 to 30 mol% of additional carbon, respectively. Increasing bias potential leads to a decrease of the growth rate from 40 to 31 nm/min, for the pure WC-target between floating and −100 V, and a decrease from 52 to 41 nm/min for WC/C (70/30) between floating and −200 V. As for carbides the carbon to metal ratio and the content of amorphous carbon in the thin films are very crucial, we determined these two properties by XPS summarized in Fig. 1. For the WC target the C/W ratio at floating potential is 0.69, which is very common when sputtering a target with a C/W ratio nearly to 1. A lower amount of carbon arrives at the substrate due to scattering with heavier atoms causing the observed carbon deficiency [28]. With increasing bias potential, the composition stays relatively constant, and the content of amorphous carbon remains between 20 and 25%, see Fig. 1b. At floating potential, the C/W ratio increases to 0.88 (WC/C (90/10)) and 1.27 (WC/C (70/30)) through the additional carbon within the targets, respectively. However, when increasing the bias potential for these two C enriched target materials, there is a significant decrease of carbon within the respective coating materials – see green diamonds and open circles in Fig. 1a. For the WC/C (70/30) target the carbon content changes even by about 20 at. % between −23 V (floating potential) and −200 V. With increasing applied bias argon ions get more and more attracted to the substrate surface causing a densification of the coating but also causing re-sputtering effects. Hence, we suggest that the decrease in carbon content with increasing bias potential is dominated by re-sputtering of carbon. Furthermore, surface diffusion is also strongly influenced by the bias potential playing an important role for the composition and the phase constitution of the thin films.

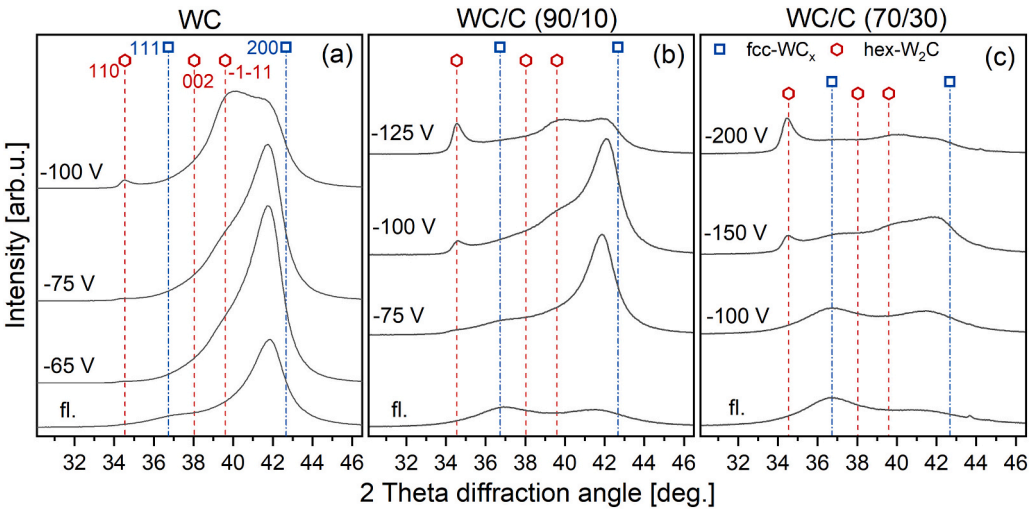

Fig. 2. Structure analysis of the coatings performed by XRD. With increasing bias potential the preferred structure changes from fcc-WC_x (SG 225) [30] to hex-W_2C (SG 162) [29] for all target types (a-c).

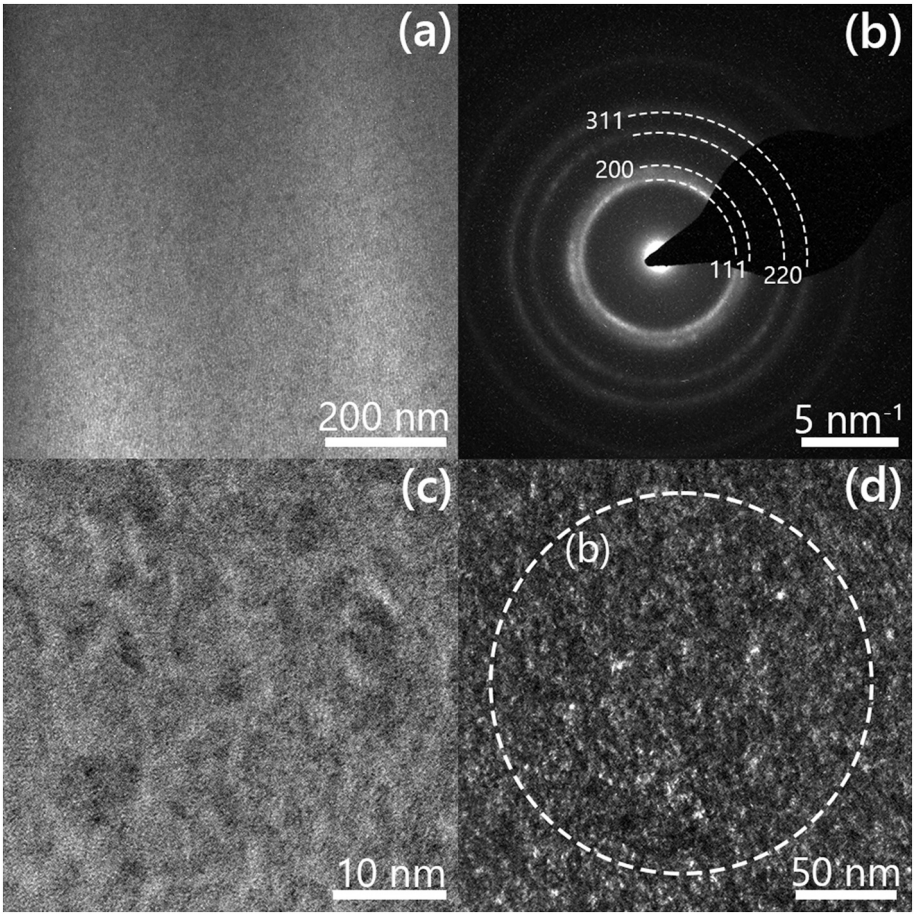

Fig. 3. TEM images of a thin film (WC/C 70/30, -100 V) obtaining a nanocrystalline morphology. The SAED image (b) exhibits circular diffraction rings corresponding to fcc-WC_x [30]. The DF image (d) further shows the nanocrystalline character. Growth direction of the coatings is from bottom to top of the images.

Nevertheless, the amount of amorphous carbon is increased for increasing additional carbon within the target, whereas for a raise in bias potential no clear trend is visible – see Fig. 1b.

As mentioned above, W—C exhibits different competing structure types in a small compositional and energetical range, hence obtaining a strong tendency to form multi-phased structures. In Fig. 2 the structural evolution for all three target materials with varying bias potentials is summarized. We observed a clear trend for all targets investigated, where fcc-WC_x accompanied by a growing content of a W_2C based phase occur with increasing bias voltage. The reference patterns of W_2C SG 162 and 60 are nearly identical, hence it was not possible to determine in detail the predominant phase. Due to simplifications, only the peak

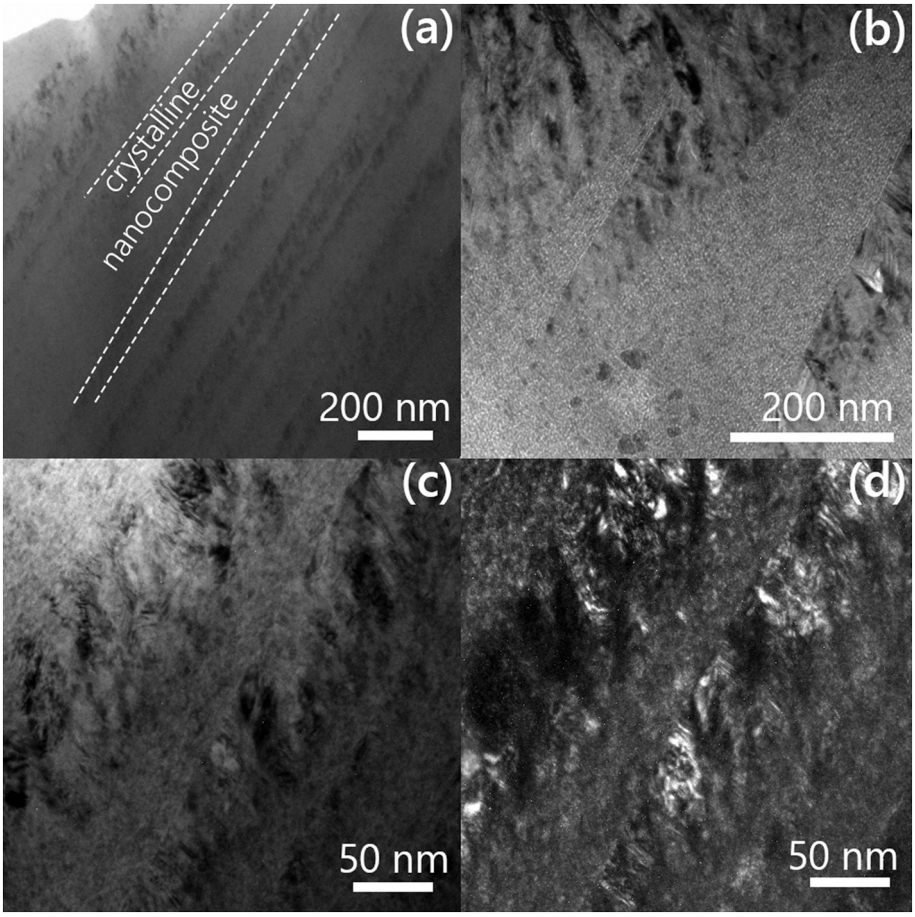

Fig. 4. TEM images of thin films (WC/C 90/10, -75 V (a,c,d) and WC/C 70/30, −150 V (b)) obtaining a mixed morphology. This morphology contains nanocrystalline areas with columnar grains in between. These columns grow in a 55° angle from the substrate coating interface. Growth direction of the coatings is from bottom to top, whereby the bottom edges of the pictures are aligned parallel to the substrate surface.

positions of hex-W_2C SG 162 [29] are indicated in Fig. 2. In general, all patterns exhibit peak broadening with increasing additional carbon. Furthermore, the amount of W_2C present also correlates with increasing bias potential. This is especially pronounced when comparing coatings from the WC and the WC/C (70/30) target. The pronounced stabilization of W_2C is in good relation to the observed change in chemistry as presented in Fig. 1. However, the same is found for the WC target where the C/W ratio is quite constant. Therefore, the changed surface mobility due to the higher bias potentials tends to have a predominant effect and will be discussed in more detail. Here, we want to mention that an increased W_2C phase fraction due to increased bias potentials is also reported in Ref. [20], where a WC target was RF sputtered in pure argon. However, this increase was only attributed to the decreased carbon content in the films.

4.2. Morphological descriptions

When correlating the XRDs with the morphology investigated by TEM, we found that not only the phase constitution changes with the bias voltage, but also the morphology. We observed three different types of morphologies being described in detail in the following. Fig. 3 shows TEM images from a sample (WC/C (70/30), -100 V) with a nanocrystalline morphology – see Fig. 3c and d. The circular diffraction rings in the SAED image (Fig. 3b) prove the nano-crystallinity of the coating but having no distinct texture as the intensity along the diffraction rings is relatively constant. This is further emphasized by the dark field image in Fig. 3d which shows randomly distributed globular crystallites. However, no detailed HR-TEM investigations were done to determine if there is an additional amorphous matrix or not, which would imply a nanocomposite morphology. From a comparison, with XRD, TEM, SAED and nanoindentation analysis in literature on W—C coatings [1,6] no completely clear assessment can be made if the coatings obtain a nanocrystalline or nanocomposite morphology. Hence, we used the more general term nanocrystalline to describe the morphology. However, a tendency towards nanocomposite is given and especially the XRD spectrum of the coating deposited using the WC/C (70/30) target at floating potential appears very similar to XRD analysis of nanocomposite coatings.

The second type of morphology is illustrated in Fig. 4 and denotes to a so-called mixed morphology. The mixed morphology is based on nanocrystalline areas with columnar grains in between – nicely shown in Fig. 4a. Interestingly, these columns all grow in a 55° angle from the substrate surface. The columns themselves consist of smaller columnar grains, but these grains do not grow in the direction of the huge column - more in a 90° mode with respect to the substrate surface (Fig. 4 c-d). We observed this morphology both for fcc-WC_x rich (WC, fl.; WC/C (90/10), −75 V) and W_2C rich coatings (WC/C (70/30), −150 V, −200 V). Considering the fcc-WC_x rich coatings, the XRD patterns exhibit a pronounced (100) texture suggesting that the smaller columnar grains grow in ⟨001⟩ direction. In a further consequence, the lattice planes having a 55° angle with respect to the (100) planes are the (111) planes. This suggests, that the (111) plane acts as preferential site for nucleation of the small grains in the column and hence leads to the 55° angle of the whole column. However, the question arises why all columns grow in the same direction. A possible explanation for that observation could be a strongly aligned deposition flux, hence preferring only the direction

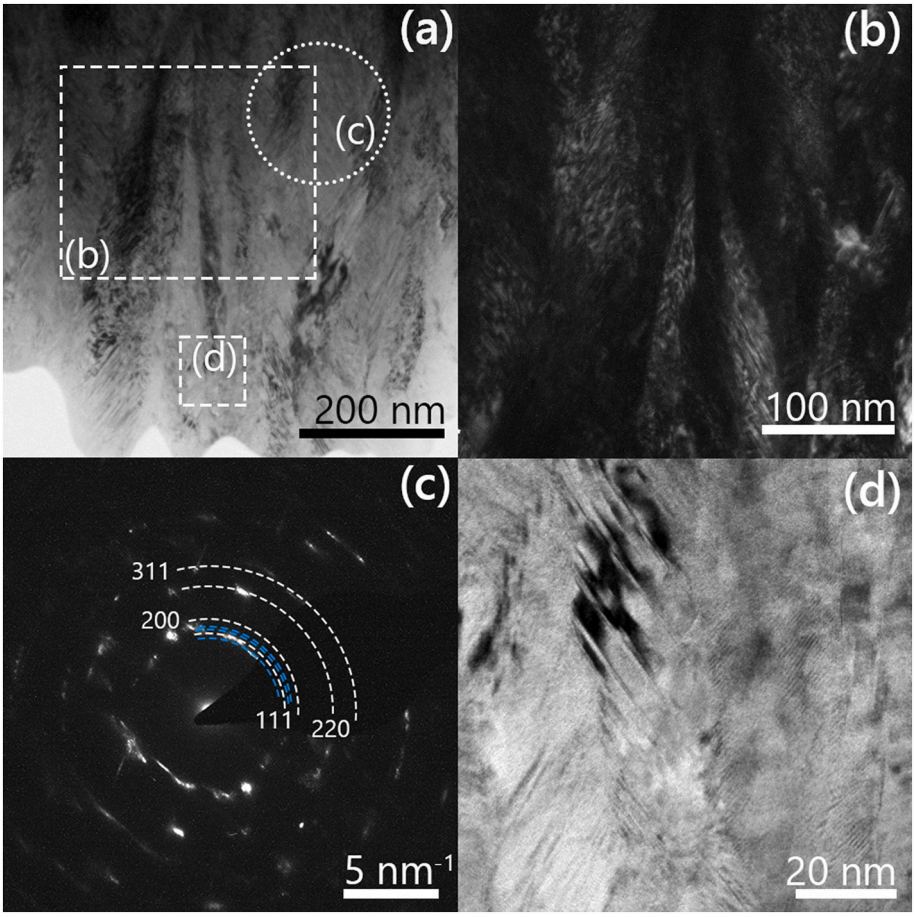

Fig. 5. TEM images of a thin film (WC, -75 V) obtaining columnar-crystalline morphology. The dashed lines in the SAED image (c) indicate fcc-WC_x [30] (white) and hex-W_2C [29] (blue). Growth direction of the coatings is from bottom to top of the images. (For interpretation of the references to colour in this figure legend, the reader is referred to the web version of this article.)

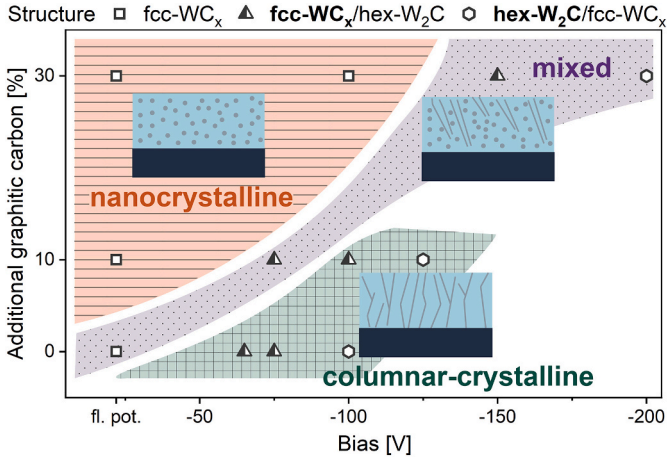

Fig. 6. Schematic illustration of resulting morphologies in dependence of the bias potential and additional amount of carbon within the target material. Orange (lines), purple (dots) and green (squared) areas represent the nanocrystalline, mixed and columnar-crystalline morphology, respectively. Symbols indicate the thin films investigated in the TEM concerning the predominant morphology. Furthermore, the symbol type indicates the observed crystal structures in the XRD pattern of the coatings (see Fig. 2). (For interpretation of the references to colour in this figure legend, the reader is referred to the web version of this article.)

closer to the direction of the deposition flux.

Finally, the third morphology features a columnar-crystalline character (Fig. 5). Here, we observed highly dense V-shaped columns. In addition, the spots in the SAED pattern are not sharp and distinct, which indicates a high concentration of structural defects and strain fields inside the columns.

Fig. 6 summarizes the different morphologies in dependence to the bias voltage and the amount of additional graphitic carbon added to the WC target (mol. %). The schematic illustrations emphasize how the different morphologies can be obtained by simply varying the bias voltage with respect to the usage of the different target materials. Orange (lines), purple (dots) and green (squared) areas represent the nanocrystalline, mixed and columnar-crystalline morphology, respectively. Here we want to mention, that for the pure WC target the mixed morphology at floating potential was only observed for very specific deposition parameters, but the coatings get easily columnar-crystalline when varying these parameters as reported in [11]. For the WC/C (90/10) target at floating potential, parameter variations did not change the nanocrystalline morphology. However, changing the bias potential a transition from the nanocrystalline to mixed to columnar-crystalline regime can be accomplished. Furthermore, variations in deposition pressure (p_{dep}) and target current at a constant bias of −75 V using the WC/C (90/10) target highlighted a further influence of p_{dep}. At a p_{dep} = 0.2 Pa increased W_2C phase fraction forms, whereas higher target currents do not influence the phase constitution. However, we want to highlight that the thin films appearing nearly single phase structured fcc are not perfectly columnar-crystalline – see Fig. 2. The formation of nanocrystalline domains is also visible for the pure WC target at floating

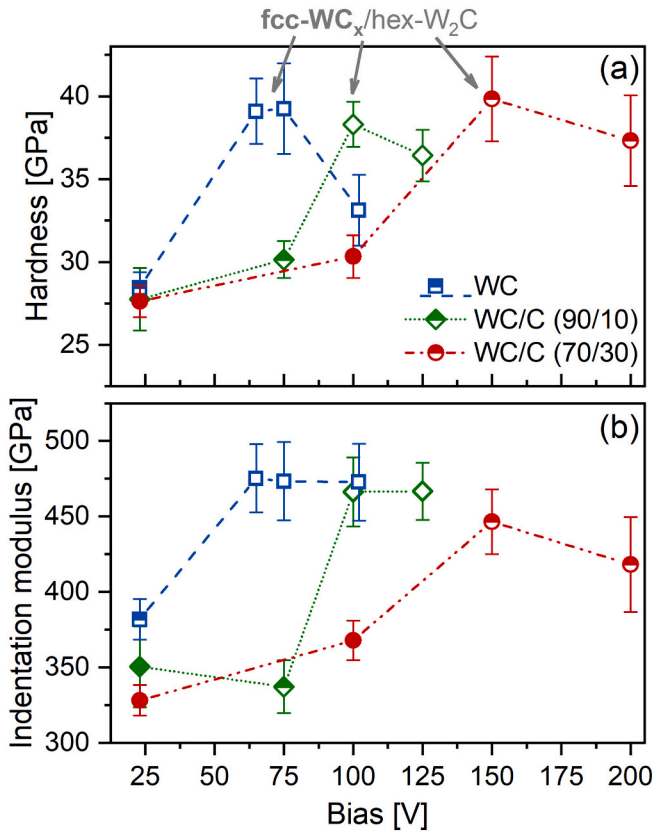

Fig. 7. Mechanical properties of the thin films obtained by nanoindentation. There is a large hardness and indentation modulus increase with increasing bias which we attribute to the changed morphology. Filled symbols label nanocrystalline coatings, half-filled symbols mixed morphology and open symbols columnar-crystalline coatings, respectively.

potential. Using a highly carbon rich WC/C (70/30) target, no predominantly columnar-crystalline morphologies could be deposited. Based on the observed results, a proper strategy to stabilize columnar-crystalline coatings being single phase fcc-WC_x structured is to go along the bias transition line between a mixed and columnar-crystalline morphology. Furthermore, the results suggest that this is best feasible using the WC/C (90/10) target, where the transition is between −75 and − 100 V bias for the used deposition parameters.

4.3. Mechanical properties

In Fig. 7 the influence of the bias potential on the mechanical properties – and hence, on the morphology and structure – is summarized. The different morphologies are labelled through open (columnar-crystalline), half-filled (mixed), and full (nanocrystalline) symbols respectively. Coatings with a nanocrystalline morphology exhibit hardness values between 27 and 30 GPa and an indentation modulus ranging from 330 to 370 GPa – see full symbols in Fig. 7a and b. For the mixed morphology there is quite a broad variation in hardness and indentation modulus. Whereas coatings from the WC and WC/C (90/10) target exhibit a hardness of 28.4 and 30.2 GPa respectively, coatings from the WC/C (70/30) target exhibit much higher hardness up to 39 GPa. For these two coatings TEM analysis revealed a changing morphology from the substrate to coating interface to the surface varying from predominantly nanocrystalline to crystalline columns. At very high bias voltages the individual columns are densely packed in the surface near region (see Fig. 4b at a bias of −150 V). Hence, the hardness is close to columnar-crystalline coatings and not in the range of their nanocrystalline counterparts. The denoted columnar-crystalline films

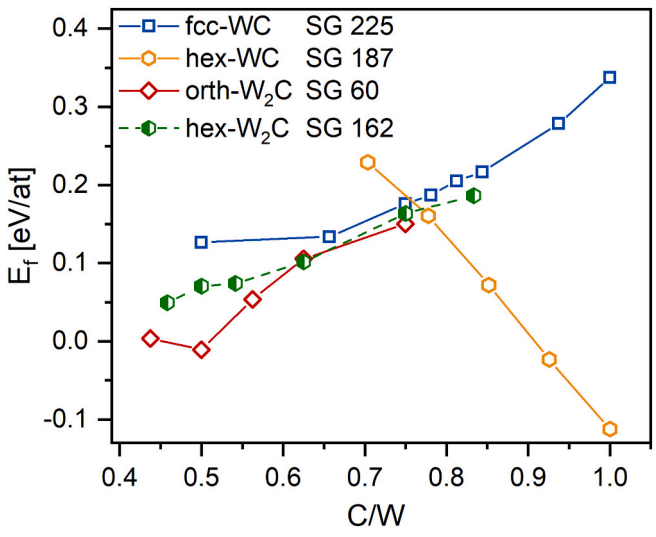

Fig. 8. Energy of formation (E_f) obtained by VASP for different W—C structures. The lower E_f the stronger is the driving force to form the specific structure.

show a similar hardness of up to 39 GPa. Interestingly the hardness decreases again when the amount of hex-W_2C phase gets prevalent, see data point at −100 V bias for the pure WC target in Fig. 7a. However, the indentation modulus stays constant at around 465 GPa. In Ref. [18] the hardness of fcc-WC and hex-W_2C are theoretically estimated to 22.25 and 24.42 GPa respectively, just considering stoichiometric structures. This suggests that the hardness drop is not simply due to a higher phase fractions of hex-W_2C, but also influenced by other factors. The large difference in hardness between nanocrystalline and columnar-crystalline further emphasizes the necessity to have a comparative picture of structure and morphology in order to fully understand structure-mechanical properties of WC based coatings.

In addition, thin films obtaining a nanocrystalline morphology obtained very low compressive stresses (around −0.5 GPa on Si substrates), which allowed us to grow additional coatings up to 12 μm thickness without any delamination or cracking.

4.4. Phase formation by DFT

To get a deeper understanding on the interplay of different crystal structures and morphologies, we additionally performed DFT calculations using VASP. Fig. 8 shows the energy of formation (E_f) for different crystal structures with varying C/W ratio. E_f was calculated after eq. (1) where E_0 denotes the total energy of the relaxed supercell that is divided by the total number of atoms in the cell. E_W and E_C are the total energy per atom of tungsten and carbon in their stable state at ambient conditions, body centered cubic W and graphite C respectively. n_W and n_C are the number of tungsten and carbon atoms in the cell.

$$E_f = E_0 - \frac{n_W E_W + n_C E_C}{n_W + n_C} \quad (1)$$

At high C/W ratios (>0.8) the hexagonal WC (SG 187) phase exhibits the lowest E_f suggesting this structure to be preferred. For very low C/W ratios the W_2C (SG 60) structure is the most stable one. In the region in between (0.65 to 0.8) the E_f of fcc-WC_x and W_2C are quite similar. When comparing these results with the obtained compositions and structures of the thin films (Fig. 1), one can see that for high C/W ratios, the coatings rather form a nanocrystalline morphology exhibiting fcc-WC_x grains, than the hex-WC, as suggested by DFT. In this study the hex-WC structure was not observed at all. If the C/W ratio ranges between 0.65 and 0.8, DFT calculations suggest that not mainly the chemistry but rather small changes in the deposition conditions e.g. surface mobility

alter the structure. If the C/W ratio is below 0.65 the composition becomes again predominant, favoring W_2C structures. The C/W ratio of all deposited columnar-crystalline coatings ranges between 0.65 and 0.8. This suggests, that the increased W_2C phase fractions observed for higher bias potentials are due to increased adatom mobility rather than the small decrease of the C/W ratio. This is further emphasized by the observation of a low Ar pressure leading to a higher W_2C phase fractions. Lower Ar pressure promotes higher mean free path, hence the incoming atoms exhibit an increased energy pushing the structure again to the most stable state. Nevertheless, the E_f of all compounds (except stoichiometric hex-WC) is relatively high, hence the tendency to form columnar-crystalline WC structures in general is limited. This also supports the observation of easily formed nanocrystalline morphologies for tungsten carbide thin films.

5. Conclusion

Within this study, the influence of additional carbon in WC based target materials as well as the bias potential on structure-mechanical properties of WC coatings is investigated in detail.

Next to varied target compositions (pure WC, WC/C 90/10 mol% as well as WC/C 70/30 mol%) leading to an increase in carbon content up to $WC_{1.27}$, the C/W ratio within the films is especially influenced by high bias potentials (above −80 V for carbon rich targets). The prevalent surface mobility, caused by bias, also changes the morphology from nanocrystalline to highly columnar crystallites with an intermediate mixed morphology between these two states. Furthermore, the observed columnar-crystalline coatings undergo a transition from fcc-WC_x to W_2C rich structures with increasing bias potential. The bias needed to cause the transition rises with increasing additional carbon within the target material – no columnar-crystalline morphology was observed using 30 mol% C containing targets. The mechanical properties vary significantly for the different morphologies. Lowest hardness was observed for nanocrystalline coatings (27 GPa), whereas highest hardness is achieved for films with densely packed crystalline grains (at least in the surface near region) (39 GPa). Additional, DFT calculations provided a more detailed insight into the tungsten carbide phase formation, suggesting not only the chemical composition being predominant during phase formation but also small changes in the adatom mobility.

In summary, this study offers an effective way for tuning the structure-mechanical properties of WC based films by adding additional carbon to WC based target materials and secondly varying the bias potential.

CRediT authorship contribution statement

T. Glechner: Conceptualization, Software, Investigation, Writing - Original Draft.

C. Tomastik: Investigation.

E. Badisch: Resources.

P. Polcik: Resources, Writing - Review & Editing.

H. Riedl: Supervision, Conceptualization, Writing - Review & Editing.

Declaration of competing interest

The authors declare that they have no known competing financial interests or personal relationships that could have appeared to influence the work reported in this paper.

Acknowledgements

We thank the financial support of Plansee Composite Materials GmbH. This work was funded by the Austrian COMET Program (project K2 InTribology1, no. 872176) and partly carried out at the “Excellence Centre of Tribology” AC2T research GmbH. In addition, we want to thank the X-ray center (XRC) of TU Wien for beam time as well as the electron microscopy center - USTEM TU Wien - for using the SEM and TEM facilities. The authors acknowledge TU Wien Bibliothek for financial support through its Open Access Funding Programme. The computational results presented have been achieved using the Vienna Scientific Cluster (VSC).

References

[1] A. Czyzniewski, Deposition and some properties of nanocrystalline WC and nanocomposite WC/aC: H coatings, Thin Solid Films 433 (2003) 180–185.
[2] K.A. Kuptsov, A.N. Sheveyko, E.I. Zamulaeva, D.A. Sidorenko, D.V. Shtansky, Two-layer nanocomposite WC/a-C coatings produced by a combination of pulsed arc evaporation and electro-spark deposition in vacuum, Mater. Des. 167 (2019), https://doi.org/10.1016/j.matdes.2019.107645.
[3] D. He, W. Li, L. Wang, Z. Lu, G. Zhang, Z. Cai, Impact wear behavior of WC/a-C nanomultilayers, Mater. Res. Express 6 (2019), https://doi.org/10.1088/2053-1591/ab4d29.
[4] D. He, Y. Zhao, W. Li, L. Shang, L. Wang, G. Zhang, Superior mechanical and tribological properties governed by optimized modulation ratio in WC/a-C nano-multilayers, Ceram. Int. 47 (2021) 16861–16869.
[5] M. Stüber, H. Leiste, S. Ulrich, H. Holleck, D. Schild, Microstructure and properties of low friction TiCC nanocomposite coatings deposited by magnetron sputtering, Surf. Coat. Technol. 150 (2002) 218–226.
[6] M.A. Abad, S.El Muñoz-Márquez, A. Mrabet, J.C. Justo, Sánchez-López, tailored synthesis of nanostructured WC/a-C coatings by dual magnetron sputtering, Surf. Coat. Technol. 204 (2010) 3490–3500.
[7] R. Hauert, J. Patscheider, From alloying to nanocomposites—improved performance of hard coatings, Adv. Eng. Mater. 2 (2000) 247–259.
[8] U. Jansson, E. Lewin, M. Råsander, O. Eriksson, B. André, U. Wiklund, Design of carbide-based nanocomposite thin films by selective alloying, Surf. Coat. Technol. 206 (2011) 583–590.
[9] D. Galvan, Y.T. Pei, J.T.M. De Hosson, Influence of deposition parameters on the structure and mechanical properties of nanocomposite coatings, Surf. Coat. Technol. 201 (2006) 590–598.
[10] Y.T. Pei, D. Galvan, J.T.M. De Hosson, Nanostructure and properties of TiC/a-C: H composite coatings, Acta Mater. 53 (2005) 4505–4521.
[11] T. Glechner, R. Hahn, L. Zauner, S. Rißlegger, A. Kirnbauer, P. Polcik, H. Riedl, Structure and mechanical properties of reactive and non-reactive sputter deposited WC based coatings, J. Alloys Compd. 885 (2021), 161129.
[12] A.A. Voevodin, J.P. O'Neill, S.V. Prasad, J.S. Zabinski, Nanocrystalline WC and WC/a-C composite coatings produced from intersected plasma fluxes at low deposition temperatures, J. Vac. Sci. Technol. A: Vac. Surf. Films 17 (1999) 986–992.
[13] P. Gouypailler, Y. Pauleau, Tungsten and tungsten-carbon thin-films deposited by magnetron sputtering, J. Vac. Sci. Technol. A: Vac. Surf. Films 11 (1993) 96–102.
[14] L. Wang, L. Li, X. Kuang, Effect of substrate bias on microstructure and mechanical properties of WC-DLC coatings deposited by HiPIMS, Surf. Coat. Technol. 352 (2018) 33–41.
[15] K. Fuchs, P. Rödhammer, E. Bertel, F.P. Netzer, E. Gornik, Reactive and non-reactive high rate sputter deposition of tungsten carbide, Thin Solid Films 151 (1987) 383–395.
[16] E. Eser, R.E. Ogilvie, K.A. Taylor, The effect of bias on d.C. And r.F. Sputtered WC-co coatings, Thin Solid Films 67 (1980) 265–277.
[17] A. Cavaleiro, M.T. Vieira, G. Lemperière, Structure and chemical composition of W-C-(Co) sputtered films, Thin Solid Films 197 (1991) 237–255.
[18] Y. Li, Y. Gao, B. Xiao, T. Min, Z. Fan, S. Ma, L. Xu, Theoretical study on the stability, elasticity, hardness and electronic structures of W-C binary compounds, J. Alloys Compd. 502 (2010) 28–37.
[19] E.C. Weigert, M.P. Humbert, Z.J. Mellinger, Q. Ren, T.P. Beebe, L. Bao, J.G. Chen, Physical vapor deposition synthesis of tungsten monocarbide (WC) thin films on different carbon substrates, J. Vac. Sci. Technol. A 26 (2008) 23–28.
[20] J.E. Krzanowski, J.L. Endrino, The effects of substrate bias on phase stability and properties of sputter-deposited tungsten carbide, Mater. Lett. 58 (2004) 3437–3440.
[21] U. Jansson, E. Lewin, Sputter Deposition of Transition-metal Carbide Films - A Critical Review From a Chemical Perspective, 2013.
[22] H. Lasfargues, T. Glechner, C.M. Koller, V. Paneta, D. Primetzhofer, S. Kolozsvári, D. Holec, H. Riedl, P.H. Mayrhofer, Non-reactively sputtered ultra-high temperature hf-C and ta-C coatings, Surf. Coat. Technol. 309 (2017) 436–444.
[23] G.M. Pharr, An improved technique for determining hardness and elastic modulus using load and displacement sensing indentation experiments, J. Mater. Res. 7 (1992) 1564–1583.
[24] G. Kresse, J. Furthmüller, Efficient iterative schemes for ab initio total-energy calculations using a plane-wave basis set, Phys. Rev. B Condens. Matter 54 (1996) 11169–11186.
[25] G. Kresse, D. Joubert, From ultrasoft pseudopotentials to the projector augmented-wave method, Phys. Rev. B Condens. Matter 59 (1999) 1758–1775.
[26] J.P. Perdew, K. Burke, M. Ernzerhof, Generalized gradient approximation made simple, Phys. Rev. Lett. 77 (1996) 3865–3868.
[27] S. Wei, L.G. Ferreira, J.E. Bernard, A. Zunger, Electronic properties of random alloys: special quasirandom structures, Phys. Rev. B Condens. Matter 42 (1990) 9622–9649.

[28] H. Riedl, T. Glechner, T. Wojcik, N. Koutná, S. Kolozsvári, V. Paneta, D. Holec, D. Primetzhofer, P.H. Mayrhofer, Influence of carbon deficiency on phase formation and thermal stability of super-hard TaCy thin films, Scr. Mater. 149 (2018) 150–154.

[29] International Center of Diffraction Data, Powder Diffraction File 04-014-5679, 2019.

[30] International Center of Diffraction Data, Powder Diffraction File 04-022-5716, 2019.